coatings

MDPI

Article

Titanium Dioxide Coatings Doubly-Doped with Ca and Ag Ions as Corrosion Resistant, Biocompatible, and Bioactive Materials for Medical Applications

Barbara Burnat [1,*], Patrycja Olejarz [2], Damian Batory [3], Michal Cichomski [4], Marta Kaminska [5] and Dorota Bociaga [6]

1 Department of Inorganic and Analytical Chemistry, Faculty of Chemistry, University of Lodz, 12 Tamka St., 91-403 Lodz, Poland
2 Department of Environmental Chemistry, Faculty of Chemistry, University of Lodz, 163 Pomorska St., 90-236 Lodz, Poland; patrycja.olejarz@o2.pl
3 Department of Vehicles and Fundamentals of Machine Design, Faculty of Mechanical Engineering, Lodz University of Technology, 1/15 Stefanowskiego St., 90-924 Lodz, Poland; damian.batory@p.lodz.pl
4 Department of Materials Technology and Chemistry, Faculty of Chemistry, University of Lodz, 163 Pomorska St., 90-236 Lodz, Poland; michal.cichomski@chemia.uni.lodz.pl
5 Division of Biophysics, Faculty of Mechanical Engineering, Lodz University of Technology, 1/15 Stefanowskiego St., 90-924 Lodz, Poland; marta.kaminska@p.lodz.pl
6 Division of Biomedical Engineering and Functional Materials, Faculty of Mechanical Engineering, Lodz University of Technology, 1/15 Stefanowskiego St., 90-924 Lodz, Poland; dorota.bociaga@p.lodz.pl
* Correspondence: barbara.burnat@chemia.uni.lodz.pl; Tel.: +48-426-355-800

Received: 27 December 2019; Accepted: 8 February 2020; Published: 13 February 2020

Abstract: The aim of this study was to develop a multifunctional biomedical coating that is highly corrosion resistant, biocompatible, and reveals the bioactive properties. For that purpose, titanium dioxide coatings doubly-doped with Ca and Ag ions were deposited by dip-coating onto M30NW biomedical steel. The influence of different ratios of Ca and Ag dopants on morphology, surface structure, corrosion resistance, bioactivity, wettability, and biological properties of TiO_2-based sol-gel coatings was studied and discussed. Comprehensive measurements were performed including atomic force microscopy (AFM), scanning electron microscopy (SEM), X-ray diffraction (XRD), X-ray reflectivity (XRR), corrosion tests, immersion test, contact angle, as well as biological evaluation. The obtained results confirmed that anatase-based coatings containing Ca and Ag ions, independently of their molar ratio in the coating, are anticorrosive, hydrophilic, and bioactive. The results of the biological evaluation indicated that investigated coatings are biocompatible and do not reduce the proliferation ability of the osteoblasts cells.

Keywords: sol-gel coating; corrosion resistance; cells viability; biocompatibility; hydrophilic coating

1. Introduction

Metallic biomaterials as materials implanted into a living system must fulfill stringent requirements, including good corrosion resistance, mechanical properties, and biocompatibility. Nowadays, studies on orthopedic biomaterials are focused mainly on enhancing their bioactivity and giving them new properties (e.g., antibacterial properties). It is well known that antimicrobial biomaterials prevent post-operative infections by reducing the ability of adhesion and permanent attachment of microorganisms and thus the development of biofilm, which is the main reason for the infections. Within the numerous methods used for the preparation of biomaterials with the desired properties, covering their surfaces with functionalized coatings appears to be particularly interesting with high capabilities.

Titanium dioxide is one of most interesting materials, which can be applied as a coating of biomaterial. It is a hard, corrosion resistant, and well biocompatible material with UV-induced hydrophilicity [1]. Literature studies show that several techniques for titanium dioxide coatings preparation, such as thermal and electrochemical oxidation (in case of titanium substrates) [2,3], magnetron sputtering [4,5], chemical vapor deposition [6–9], and sol-gel [2,7,10–13] have been investigated. But one of the most frequently used methods is sol-gel due to its high application potential [14]. The sol-gel TiO_2 coating was proven to be a versatile platform for surface functionalization of stainless steels and other biomedical metals. The desired properties of the biomaterial can be obtained by careful control of sol-gel reaction conditions or by the use of suitable additives. One of the possibilities is to improve biocompatibility, bioactivity (related to osseointegration), and antibacterial properties of biomaterials by means of ion doping procedure. In the literature, there are reports about enhanced bioactivity of TiO_2 coating by means of incorporation of Ca [15,16], Mg [17] and Sr [18,19] ions. Our previous papers [20,21] also confirmed improved bioactivity of Ca-doped TiO_2 sol-gel coatings. It was also proved that, in an analogous manner, the antibacterial properties may be achieved by doping of bactericidal molecules that in most cases have antibacterial properties per se, namely Ag ions/nanoparticles [22–24], Cu ions [25,26], and Zn ions [27]. Several research studies [28–30] have shown that F doping enhances the antibacterial properties of TiO_2 too. However, studies on the biocompatibility of the fluoride-modified surface have contradictory and inconclusive results. A very interesting idea is to obtain a multifunctional coating in a co-doping procedure [31–33]. In the present study, we applied the possibility of incorporating more than one modifier into the sol solution in order to achieve a multifunctional biomedical coating with bioactive and antibacterial behavior, and what is the most important exhibiting corrosion protection capability towards biomedical stainless steels. We intended to combine anticorrosion properties of titanium dioxide with the bioactive effect of Ca ions and the potential antibacterial effect of Ag ions widely reported in the literature. In the literature, there are reports on TiO_2 coatings co-doped with Ca and Ag ions [34,35], but those coatings were applied to titanium rather than steel substrates, and deposition methods other than sol-gel were used. However, since the method chosen for coating preparation or its modification determines the final properties as well as the applicability of the biomaterial, we have to remember that the improvement of a certain feature or function of a biomaterial as a result of surface modification may be accompanied by deterioration of other biomaterial features. Yetim et al. reported, for example, that, using plasma nitriding, it was possible to improve the wear resistance of AISI 316L steel, but the nitriding treatment did not bring the expected improvement in the corrosion resistance of the AISI 316L steel, it was even worse [36]. Junping et al. stated that the Ce-modified 316L steel exhibits the hormesis effect against *Staphylococcus aureus* (the higher the Ce content, the better the antibacterial efficacy), but it is difficult to simultaneously obtain good corrosion resistance, antibacterial performance, and processability [37]. Based on these literature examples, it is clear how important it is to control the impact of carried out modifications on corrosion resistance, especially in the case of biomaterials, as it determines their biocompatibility.

The aim of this study was to develop a multifunctional biomedical sol-gel coating that is highly corrosion resistant, biocompatible, and reveals the bioactive properties. For that purpose, titanium dioxide coatings doubly-doped with Ca and Ag ions were deposited by dip-coating onto M30NW biomedical steel, and subsequently annealed at 450 °C in air. Our previous studies have shown that under these thermal oxidation conditions an effective crystallization of titanium dioxide occurs, and formed anatase exhibits good corrosion protection ability in case of biomedical steels [21]. In the presented study, the influence of different ratios of Ca and Ag dopants on morphology, surface structure, corrosion resistance, bioactivity, wettability, and biological properties of the TiO_2-based coating was investigated.

2. Materials and Methods

2.1. Samples' Preparation

Commercially available M30NW biomedical alloy (AUBERT & DUVAL, Paris, France), with composition and properties specified by X4CrNiMnMo21-9-4 standard, was used as a substrate. The alloy plates (22 mm in diameter) were ground with SiC papers down to 1200 grits, polished with alumina slurry (0.3 μm), ultrasonically cleaned in distilled water, etched in acid mixture, passivated in boiling distilled water, rinsed with ethanol, and dried with argon according to the procedure described elsewhere [38].

In this study several sols were used for surface modification of M30NW alloy: TiO_2 sol without dopants, sol doped with calcium ions Ca^{2+}, sol doped with silver ions Ag^+, as well as sols containing both Ca^{2+} and Ag^+ ions in different molar ratios (Ca/Ag 3:1, 1:1, 1:3).

All sols were synthesized using the sol-gel method, in which titanium tetrabutoxide (TiBut, $Ti[O(CH_2)_3CH_3]_4$, 97%, Sigma-Aldrich) was used as a precursor for titania, ethanol (EtOH, C_2H_5OH, pure p.a., 96%, POCh) as a solvent, nitric acid (HNO_3, pure p.a., 65%, POCh) as a catalyst, calcium nitrate ($Ca(NO_3)_2$ $4H_2O$, pure, CHEMPUR) and silver nitrate ($AgNO_3$, pure p.a., POCh) solutions at a concentration of 2.056 mol/L as dopant sources. The composition of all sol solutions used in this study is presented in Table 1.

Table 1. Composition of sol solutions used for surface modification of M30NW alloy.

Coating	TiBut [mL]	EtOH [mL]	HNO_3 [mL]	H_2O [mL]	$Ca(NO_3)_2$ [mL]	$AgNO_3$ [mL]	Ca/Ag Ratio
TiO_2	7	20	0.64	0.5	–	–	–
Ca_TiO_2	7	20	0.64	–	0.500	–	–
75Ca25Ag_TiO_2	7	20	0.64	–	0.375	0.125	3:1
50Ca50Ag_TiO_2	7	20	0.64	–	0.250	0.250	1:1
25Ca75Ag_TiO_2	7	20	0.64	–	0.125	0.375	1:3
Ag_TiO_2	7	20	0.64	–	–	0.500	–

A titania-based coating (as a single layer) was applied onto the alloy surface with the dip-coating technique using a DCMono 75 dip-coater (NIMA Technology Ltd., Coventry, UK). The substrate was immersed in the sol for 30 s and withdrawn at a speed of 20 mm/min. Such modified alloy samples were dried in the oven at 100 °C for 2 h and then annealed at 450 °C for 1 h.

2.2. Surface Characterization

Each type of sample was characterized in terms of surface properties. A metallographic microscope MMT 800 BT (Mikrolab, Lublin, Poland) was used for preliminary assessment of the sol-gel coatings' quality, including detection of cracks and defects. An atomic force microscope (AFM) Dimension Icon (Bruker, Santa Barbara, CA, USA) was applied for investigation of surface topography and roughness of the prepared coatings within a scan size of 1 μm × 1 μm. The AFM measurements were made in tapping mode using standard silicon probes (TESPA, Bruker AFM Probes, Camarillo, CA, USA). The morphology of the samples was observed using a field emission scanning electron microscope (FE-SEM, FEI Nova NanoSEM 450 with EDS analyzer, Thermo Fisher Scientific, Hillsbro, OR, USA), operating with an accelerating voltage of 15 kV. The phase composition and thickness of prepared coatings were identified using an Empyrean X-ray diffractometer (XRD, PANalytical, Malvern, UK) working with Cu Kα radiation (λ = 0.15418 nm). The phase analysis was carried out using GIXRD (grazing incidence X-ray diffraction) mode with an incident beam angle of 0.3°, whereas the thickness was estimated with the use of X-ray reflectivity method (XRR). Further data processing was performed using HighScore Plus with ICDD PDF 4+ Database and X'Pert Reflectivity software with Fourier transform analysis, respectively.

2.3. Corrosion Tests

The anticorrosion ability of prepared coatings was evaluated by electrochemical measurements in phosphate buffered saline (PBS, NaCl 8.0 g/L, KH_2PO_4 0.2 g/L, Na_2HPO_4 ·12 H_2O 2.9 g/L, KCl 0.2 g/L, pH 7.4) solution using a PGSTAT 30 potentiostat-galvanostat (EcoChemie Autolab, Utrecht, The Netherlands). All electrochemical experiments were performed at 37 °C, similar to human body temperature. Degassing of the electrolyte was achieved by argon bubbling through the solution. A conventional three-electrode cell was used with a platinum gauze as a counter electrode, a saturated calomel electrode (SCE, E = 0.236 V_{SHE}) as a reference, and sample with an exposed area of 0.64 cm^2 as a working electrode.

In order to establish the corrosion potential E_{cor}, each sample was kept in PBS solution (under open circuit conditions) for 2000 s. The linear polarization measurements were performed in a scanning range of ±20 mV versus E_{cor} potential, with a scan rate of 0.166 mV/s. Potentiodynamic polarization tests were conducted with a scan rate of 1 mV/s from the initial potential of −200 mV versus E_{cor} to the potential at which current density of 5 mA/cm^2 was reached, then, the potential sweep was reversed and the backward branch was registered up to the initial potential. The surface morphology of the samples after potentiodynamic polarization was analyzed using scanning electron microscopy in order to determine the type and scale of corrosion damage.

The results of linear polarization measurements and potentiodynamic polarization tests were analyzed using CorrView software (Scribner Associates Inc., Southern Pines, NC, USA) and several corrosion parameters were determined: Polarization resistance, R_p; corrosion rate, CR; pitting potential, E_{pit}; and repassivation potential, E_{rep}. Triplicate measurements were conducted to check the reproducibility of the results. Each data point presented here is given as mean ± standard deviation (SD). All the potentials reported here are with respect to a saturated calomel electrode.

2.4. Immersion Tests

To evaluate the bioactivity (as apatite formation ability) of the M30NW samples with prepared titania-based coatings, the immersion tests in a simulated body fluid (SBF) solution were carried out according to the procedure reported by Kokubo [39]. The samples were immersed in SBF (at 37 °C, similar to human body temperature) for 28 days, the solution was renewed every week. Then the SEM-EDS technique was employed to characterize the morphology and surface composition of samples. Based on SEM-EDS results, their ability to apatite formation was evaluated.

2.5. Wettability

Measurements of contact angle of M30NW alloy samples modified with TiO_2-based coatings were carried out using the DSA25 Drop Shape Analyzer goniometer- (Krüss GmbH, Hamburg, Germany). Each time, the measurement was performed for a minimum of three drops of water at an ambient temperature of approximately 20 ± 2 °C. The amount of deionized water drops applied by microsyringe was 5 μL. The values of the contact angle were determined using Advance software.

The surface free energy values were calculated based on two polar liquids-water and glycerine, and one apolar liquid-diiodomethane. Calculations were performed using van Oss Chaudhury–Good method.

2.6. Biological Evaluation (Cell Viability Assays)

Before biological evaluation, all samples were cleaned in ethanol and ultrapure water (0.055 μS/cm) for 10 min using ultrasonic cleaner. Then the steam sterilization was performed (121 °C, 31 min) using an autoclave. In order to conduct the biocompatibility assessment of the samples, the cell viability and proliferation assays were conducted. The human osteoblast cell line Saos-2 (ATCC, Manassas, VA, USA) was selected as a biological material for this purpose. Saos-2 cells were grown in McCoy's 5A medium (ATCC, Manassas, VA, USA) containing 15% fetal bovine serum (Biological Industries),

100 units/mL penicillin and 50 µg/mL streptomycin (Biological Industries). Cells were cultured in standard conditions (37 °C, humidified atmosphere of 5% CO_2 in air) and medium was replaced every 2–3 days (75% confluence). Cells were used between passages 5 and 8.

For the evaluation of proliferation and cytotoxicity marking method, a "live/dead" test (Viability/Cytotoxicity Kit, Molecular Probes) was applied. Cells were seeded at 6×10^4 cells/mL/well/sample in 2 mL of McCoy's 5A medium (ATCC, Manassas, VA, USA) and cultured for 48 h. After that time, a mixture of two fluorescent dyes was used. One of the fluorescent dyes within the live cells produces an intense uniform green fluorescence and the second one, when the membranes are damaged, penetrates the cells and binds to nucleic acids, thereby producing a bright red fluorescence in dead cells. The samples were examined in a fluorescence microscope Olympus GX 71 equipped with a digital camera (DP70).

The obtained results were analyzed by one-way ANOVA analysis with a significance level of $p < 0.05$. Statistical analysis was performed using OriginPro 9 software.

3. Results and Discussion

3.1. Surface Characterization

All prepared TiO_2-based coatings were blue in color, homogeneous, without any cracks on the surface, and they exhibited good adhesion to the substrate. Surface characterization carried out with scanning electron microscopy revealed fine crystalline structure of all TiO_2-based coatings (results not shown). In case of coatings doped with silver ions, SEM analysis revealed small white points on the surface, of which the amount was increasing with increasing concentration of silver. The SEM method does not allow conclusions to be drawn about the convexity or concavity of the surface elements, thus the topography of these white points was analyzed by atomic force microscopy. In addition, the AFM analysis made it possible to determine the roughness (by R_q parameter) of the synthesized coatings. Figure 1 presents the general view of the coated samples, and AFM images (scan sizes of 5 µm × 5 µm and 1 µm × 1 µm) for all types of coatings.

The AFM results (AFM 2D images and values of R_q) presented in Figure 1 are in good agreement with SEM results. For every sample, the coating is uniform and it reflects the topography of the substrate regardless of the coating composition. Based on AFM images, it can be observed that coatings are applied even inside the surface scratches. In addition, in case of coatings doped with calcium and silver ions, especially with the increasing amount of silver ions, holes appear on the surface of the coatings. These holes correspond to the white points observed on the SEM images. They are the result of the thermal decomposition of calcium nitrate and silver nitrate used in doping procedure. According to "CRC Handbook of Chemistry and Physics" edited by Lide [40], both nitrates undergo decomposition during heat treatment, but at different temperatures. Calcium nitrate tetrahydrate decomposes at a temperature of 132 °C, but this decomposition is not total, it only involves the removal of water molecules. The total thermal decomposition of alkaline earth metal nitrates leading to the formation of nitrogen dioxide undergoes at temperatures higher than 500 °C. Whereas, in the case of silver nitrate, such total decomposition undergoes at a temperature of 444 °C according to Equation (1):

$$2AgNO_3 \rightarrow 2Ag + 2NO_2 \uparrow + O_2 \uparrow . \quad (1)$$

The presence of these holes (pores) results in different coating roughness. Coatings with an increasing amount of silver ions are characterized by a greater surface development (higher R_q).

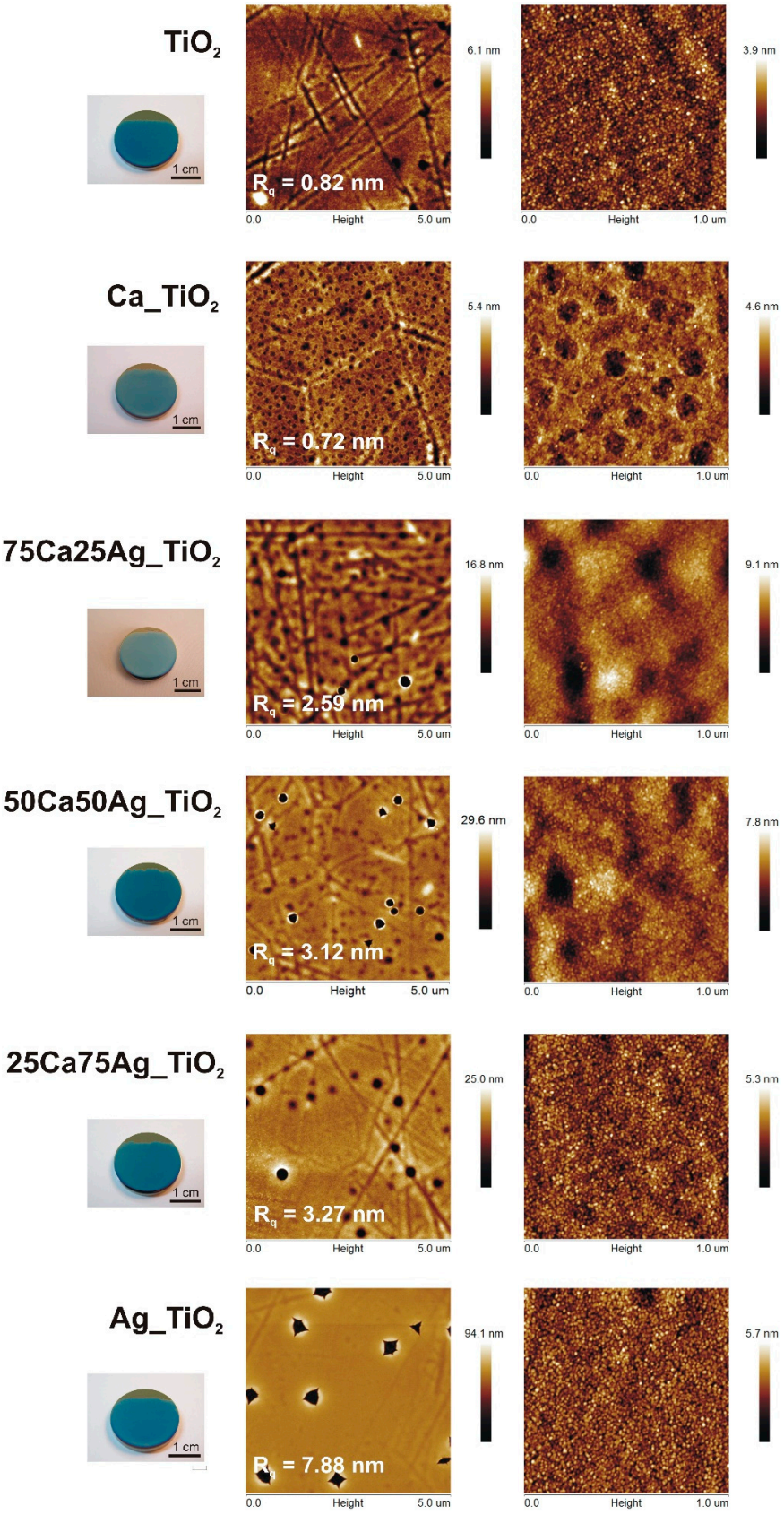

Figure 1. The general view of the coated samples, and atomic force microscopy (AFM) images (scan sizes of 5 μm × 5 μm and 1 μm × 1 μm) for all types of coatings.

The same coloration of the coatings implies similarity in the coating thickness. According to Velten et al. [2], the thickness of TiO_2 coatings that are blue in color should be in the range of 50–80 nm. The verification of this statement was performed via XRR analyses. Values of thickness of the investigated coatings were determined based on the Fourier transform analysis of the registered X-ray reflectivity curves. The obtained XRR results are presented in Table 2.

Table 2. The thickness of TiO_2-based coatings doped with Ca and Ag ions in different molar ratios.

Coating	Thickness/nm
TiO_2	77 ± 4
Ca_TiO_2	74 ± 4
75Ca25Ag_TiO_2	80 ± 4
50Ca50Ag_TiO_2	75 ± 4
25Ca75Ag_TiO_2	77 ± 4
Ag_TiO_2	78 ± 4

The determined values are in good agreement with the literature-based predictions. Furthermore, the analysis of the results allowed to conclude that if the constancy of the sol composition (the ratio of individual reagents in doping procedure) is maintained, then the doping procedure does not significantly affect the thickness of the sol-gel coating.

The phase composition of the investigated coatings was determined by X-ray diffraction method. Figure 2 shows the XRD patterns obtained for TiO_2-based coatings. The results reveal that every single coating exhibits the anatase structure of TiO_2 (Ref. 00-064-0863). This is confirmed by peaks centered at 2theta, 25.37°, broad peak being a superposition of three peaks (centered at 2theta equal to 36.93°, 37.96°, 38.64°), 48.06°, 54.02° and 55.03° (marked with asterisks on the chart). The comparison of the intensity of the peaks for particular coatings shows positive influence of silver onto the crystallization process of titanium dioxide. The most intensive and well defined peaks were registered for TiO_2 coatings with the highest concentration of silver. In the case of calcium, no noticeable difference between TiO_2 and Ca_TiO_2 XRD spectra was observed, which means the incorporated Ca does not alter the crystallization process of anatase. Therefore, it can be stated that silver promotes the crystallization of titanium dioxide in the form of anatase. Such a finding corresponds to the report of García-Serrano et al. [41].

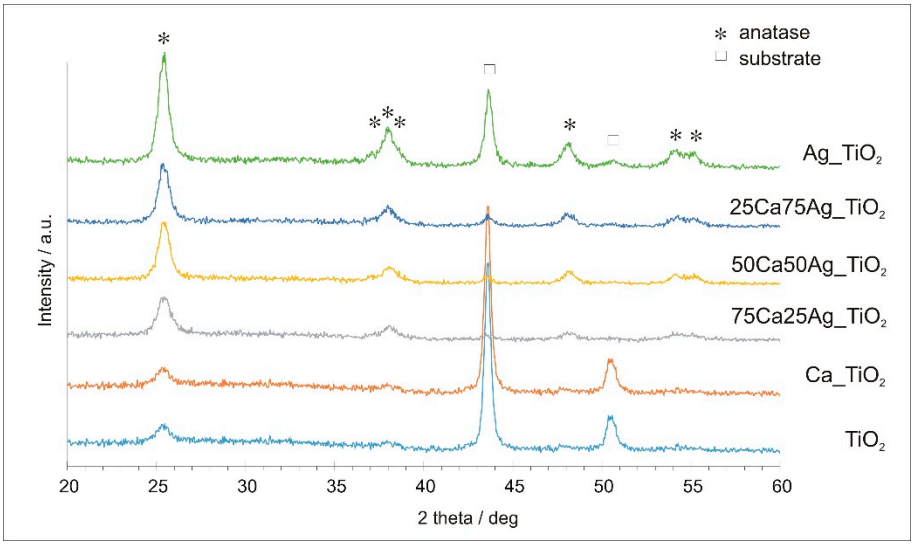

Figure 2. XRD patterns for TiO_2-based coatings doped with Ca and Ag ions in different molar ratios.

3.2. Corrosion Tests

Anticorrosion properties of TiO_2-based sol-gel coatings were determined via electrochemical methods based on polarization near the corrosion potential and polarization in wide anodic range. Such measurements allowed for the evaluation of the resistance of the samples against general and pitting corrosion in PBS solution.

The linear polarization measurements performed in a narrow scanning range (± 20 mV vs. E_{cor}), allowed for the calculation of the values of corrosion rate, CR, based on determined polarization resistance, R_p, values (according to the assumptions of standard ASTM G102-89 [42]). The mean values of E_{cor}, R_p, and CR with standard deviations for all investigated TiO_2-based coatings are given in Figure 3. In order to confirm the protective properties of TiO_2-based coatings, the results for uncoated M30NW alloy substrate are also included in Figure 3.

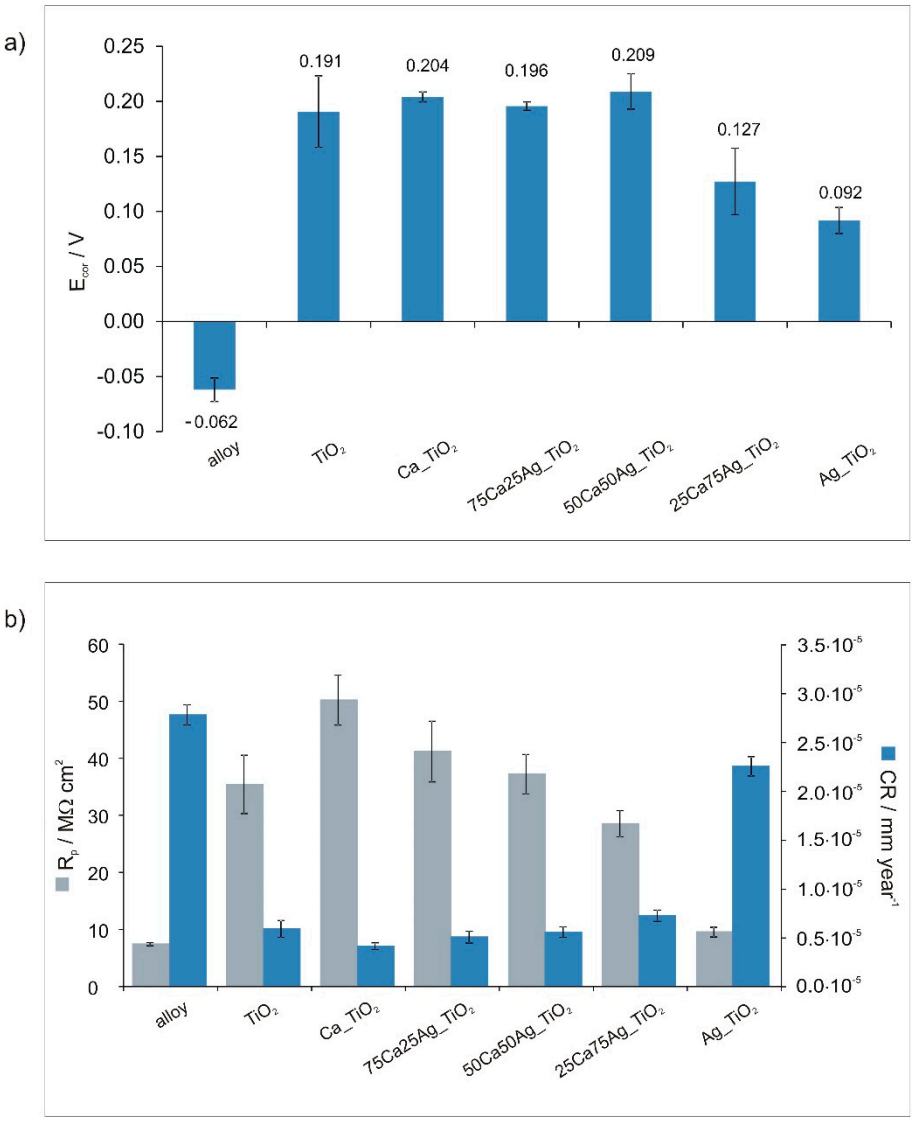

Figure 3. Values of (**a**) corrosion potential, E_{cor}, (**b**) polarization resistance, R_p, and corrosion rate, CR, determined for TiO_2-based coatings doped with Ca and Ag ions in different molar ratios.

It can be observed that the E_{cor} value remains constant (of ca. 0.20V) for undoped TiO_2 coating and coatings with predominant calcium content (i.e., Ca_TiO_2, $75Ca25Ag\_TiO_2$, $50Ca50Ag\_TiO_2$). Whereas, when the silver content is predominant and its concentration increases in the coating, the corrosion

potential progressively decreases up to 0.09V. This is attributed to the increasing amount of Ag metallic nanoparticles in the coating.

As can be seen in Figure 3b, the R_p of the Ca-doped TiO_2 coating is higher than that of the undoped TiO_2 coating, suggesting that calcium incorporation into TiO_2 coating has a significant effect in improving its corrosion resistance. However, as the silver addition in the films increases, the R_p of the coatings decreases gradually from 50 to 9.6 MΩ·cm^2. This probably means that a larger amount of silver ions is released from Ag-doped TiO_2 coatings with higher silver content, resulting in a higher corrosion rate (see CR diagram in Figure 3b). Analogous observations were reported by X. Zhang et al. [43]. While, some other researchers [24,35] reported opposite corrosion behavior of Ag-incorporated TiO_2 coatings—with an increased amount of silver content the corrosion resistance was improved. This tendency was; however, attributed to the fewer surface defects [35] or the presence of an Ag-TiO_2 nanocomposite [24]. Nevertheless, in terms of polarization resistance and corrosion rate, all our doubly-doped coatings act as corrosion protective—the samples with those coatings exhibit better corrosion resistance than the uncoated alloy substrate. According to the R_p and CR results, the Ca_TiO_2 coating provides the best anticorrosion protection for the steel substrate.

Pitting corrosion resistance of M30NW alloy samples coated with TiO_2-based coatings was examined through the potentiodynamic anodic polarization. The potentiodynamic curves of undoped TiO_2- and Ca,Ag-doped coatings were recorded in PBS solution within the wide anodic potential range (up to ca. 1.7V) in order to study the passivation and breakdown behavior of all types of coatings, and are shown in Figure 4. Table 3 gives values of corrosion quantities determined from potentiodynamic curves: current density in passive range (at arbitrary chosen potential of 0.2V) and breakdown potential E_b.

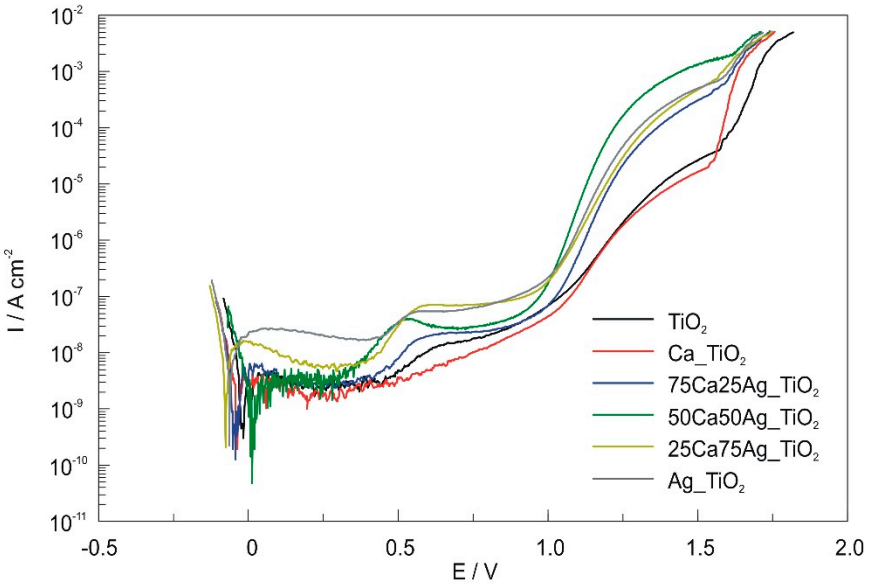

Figure 4. Potentiodynamic polarization curves of TiO_2-based coatings in phosphate buffered saline (PBS) solution (scan rate 1 mV·s^{-1}).

Table 3. Values of corrosion quantities determined from potentiodynamic characteristics.

Coating	$i_{0.2}$/nA·cm^{-2}	E_b/V
TiO_2	3.3 ± 1.1	1.600 ± 0.013
Ca_TiO_2	3.0 ± 2.2	1.524 ± 0.029
75Ca25Ag_TiO_2	3.8 ± 1.8	1.579 ± 0.024
50Ca50Ag_TiO_2	3.2 ± 3.3	1.613 ± 0.003
25Ca75Ag_TiO_2	6.2 ± 1.7	1.569 ± 0.054
Ag_TiO_2	22.9 ± 2.7	1.593 ± 0.021

Based on the potentiodynamic characteristics shown in Figure 4 and data presented in Table 3, it can be stated that an increasing amount of silver in the TiO_2 coatings results in higher electrochemical activity of the coatings. For the sample with Ca/Ag molar ratio of 1:3 (25Ca75Ag_TiO_2), the current density in passive range is two times higher when compared to the Ag-free coatings (TiO_2, Ca_TiO_2) and coatings with predominant or equal calcium content (75Ca25Ag_TiO_2, 50Ca50Ag_TiO_2). However, for the coating doped only with silver ions (Ag_TiO_2), the value of current density in the passive range is the highest, and is about 23 nA/cm^2, which is about seven times higher than for the undoped coating. This fact can be related to the previously found higher porosity of the coatings containing silver ions. The deep pores present in the coating can facilitate the penetration of the corrosion solution through the coating toward the substrate and thus increase the reactivity of the sample.

The breakdown potential E_b value was determined as the potential at which there is a sharp increase in current on the potentiodynamic curve. As shown in Figure 4 and Table 3, prepared materials are characterized by relatively high values of E_b potential of ca. 1.6 V regardless of doped ions. In order to confirm the veracity of such high E_b values, an additional experiment was also performed for each sample, and polarization was stopped at 1.5 V, just after the earlier increase in current recorded on the characteristic curve. Nevertheless, post-polarization microscopic analysis showed no pits on the surface, which proves that, in the case of investigated samples, pitting corrosion occurs at potentials higher than 1.5 V. Such high values of E_b may result from the surface finishing degree (polishing to mirror surface), passivation in mixture of HF and HNO_3 acids, as well as the nature of the titanium dioxide. Based on the corrosion tests results, it can be stated that the M30NW alloy samples with TiO_2-based coatings doped with calcium and silver ions belong to the group of high pitting corrosion-resistant materials.

On the surface of all tested TiO_2-based coatings, anodic polarization caused the formation of corrosion damages as pits, differing in morphology, depth, and width. In many cases, these pits were spherical-ish in shape and covered with corrosion sludge. Moreover, for coatings containing the addition of silver ions (75Ca25Ag_TiO_2, 50Ca50Ag_TiO_2, 25Ca75Ag_TiO_2, Ag_TiO_2), the destruction of the coating in close proximity to the pits can be observed. This is most likely the result of the greater reactivity of these samples. The SEM images shown in Figure 5 indicate that the pitting mechanism starts with the breakdown of the coating, followed by under-film corrosion (dissolution) of the substrate material. In subsequent stages, the damaged fragments of the coating wrap become detached and reveal the corroded substrate (pit). The interiors of the pits reveal the dissolved intergranular edges of the alloy grains.

3.3. Immersion Test

Studies on in vitro bone-bonding ability (referred to as bioactivity) of materials were started by Kokubo and co-workers dozens of years ago [44]. They proposed that the essential requirement for an artificial material to bond to living bone is the formation of bone-like apatite on its surface when implanted in the living body. In laboratory conditions, this ability can be assessed by immersion test in a simulated body fluid (SBF) with ion concentrations nearly equal to those of human blood plasma [39]. The evidence of the bioactive properties of the biomaterial is the formation of an apatite layer as a result of exposure to the SBF solution. Thus, an immersion test in SBF allows for the prediction of the material's in vivo bone bioactivity.

In order to study the effect of calcium and silver ions doping on bioactivity of TiO_2-based coatings, the M30NW alloy samples with five types of coatings, undoped TiO_2, Ca_TiO_2, 75Ca25Ag_TiO_2, 50Ca50Ag_TiO_2, 25Ca75Ag_TiO_2 and Ag_TiO_2, were immersed in SBF solution for 28 days, and then the samples' surfaces were examined using SEM-EDS. Figure 6 shows SEM micrographs (magnitude of 50,000×) of apatite formed on undoped TiO_2 (a), Ca_TiO_2 (b), 75Ca25Ag_TiO_2 (c), and Ag_TiO_2 (d) after soaking for 28 days in SBF solution. All these SEM images are in the same scale, thus direct comparison of the results is possible. In addition, the results of qualitative elemental analysis in the form of Ca/P molar ratios estimated for these samples are given as insets in Figure 6.

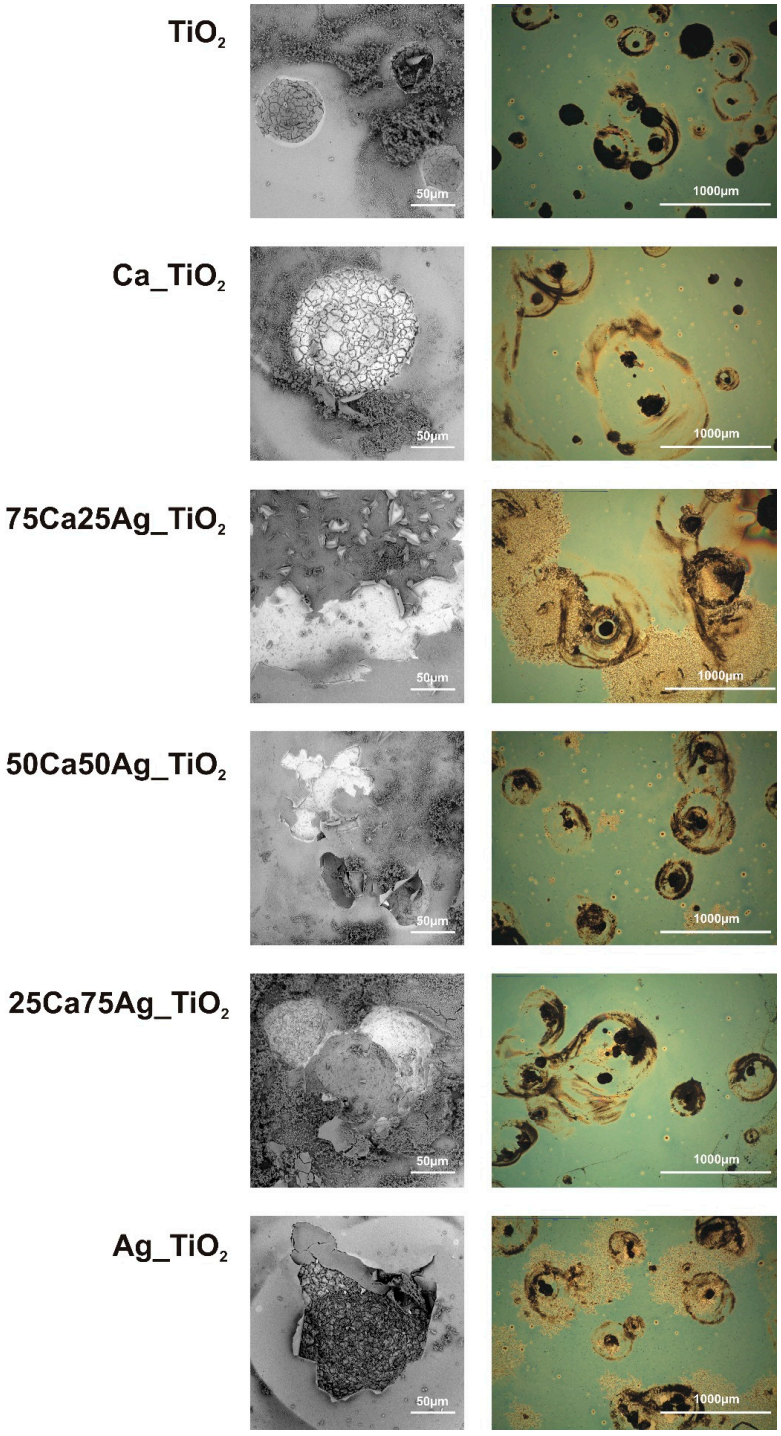

Figure 5. Post-polarization SEM images (1000× mag., bar 50 µm) and optical microscopic images (50× mag., bar 1000 µm).

SEM analysis revealed new particles of different morphologies existing on the samples' surfaces after 28 days of exposure to SBF. In case of undoped TiO_2 coating the randomly distributed agglomerates with Ca/P molar ratio of ca. 1.2 can be observed (Figure 6a). A deposit of a completely different morphology can be seen in Figure 6b for the coating doped with calcium ions (Ca_TiO_2). In this case, needle-like particles, fully covering the surface, with Ca/P molar ratio of ca. 1.5 were formed. As the content of calcium ions in the coating decreased the Ca/P ratio also decreased, and it was ca. 1.2 for $75Ca25Ag\_TiO_2$, ca. 1.2 for $50Ca50Ag\_TiO_2$, ca. 1.0 for $25Ca75Ag\_TiO_2$, and finally ca. 1.1 for Ag_TiO_2

sample. Apart from the low values of Ca/P molar ratio for coatings doped with both calcium and silver ions, the resulting deposits did not completely cover the surfaces; on the part of the surface they formed large agglomerates, while the remaining part of the surface was uncovered. The size and morphology of the particles deposited onto Ag-doped coating (Ag_TiO_2) were larger in average diameter and more interconnected comparing with undoped and Ca-Ag co-doped surfaces. No apatite aggregates were observed on Ag_TiO_2 surface.

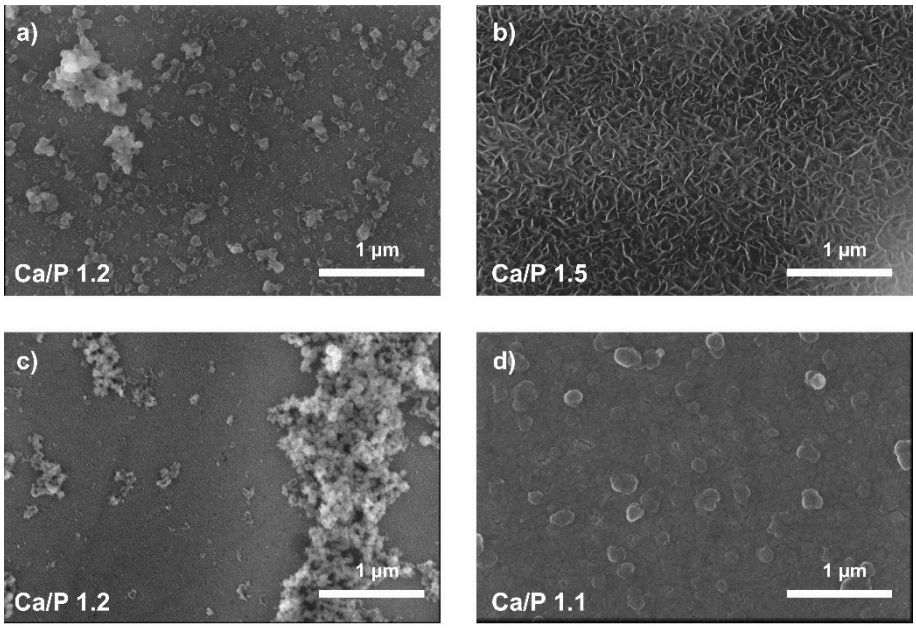

Figure 6. SEM micrographs of apatite formed on: (**a**) undoped TiO_2, (**b**) Ca_TiO_2, (**c**) $75Ca25Ag\_TiO_2$, and (**d**) Ag_TiO_2 after soaking for 28 days in simulated body fluid (SBF) solution (detector TLD, mag 50,000×, bar 1 µm).

According to Zhang et al. [45], the apatite particles nucleate spontaneously onto bioactive surfaces by consuming calcium and phosphate ions from the SBF solution (Equations (2) and (3)):

$$10Ca^{2+} + 8OH^- + 6HPO_4^{2-} \rightarrow Ca_{10}(PO_4)_6(OH)_2 + 6H_2O \quad (2)$$

$$10Ca^{2+} + 2OH^- + 6PO_4^{3-} \rightarrow Ca_{10}(PO_4)_6(OH)_2 \quad (3)$$

In case of coatings doped with calcium, the apatite nucleation is enhanced due to the presence of positively-charged calcium ions in the coating, which react with phosphate anions to form an amorphous calcium phosphate. Since this phase is metastable, it is eventually transformed into stable crystalline bone-like apatite [45]. Results obtained in this study indicate that the more Ca^{2+} that is incorporated in TiO_2 coating, the easier and quicker is the apatite nucleation on the surface. The Ca/P ratio of the apatite formed on most of the coatings fabricated in this study is in the range 1.1–1.2, which indicates that the apatites are calcium-deficient HA [33]. Only for that coating, the Ca/P ratio was approaching the value of 1.67 characteristic of the stoichiometric hydroxyapatite. It is a very important factor for orthopedic implants, since literature data indicate that the newly formed bone tissue closely adheres to the implanted element when the Ca/P molar ratio is in the range of 1.67–2.0.

3.4. Wettability

Wettability plays an important role in biological performances of materials. Hydrophilicity of the titania-based coatings on M30NW biomedical alloy samples was evaluated by measuring their water contact angles Θ (Figure 7).

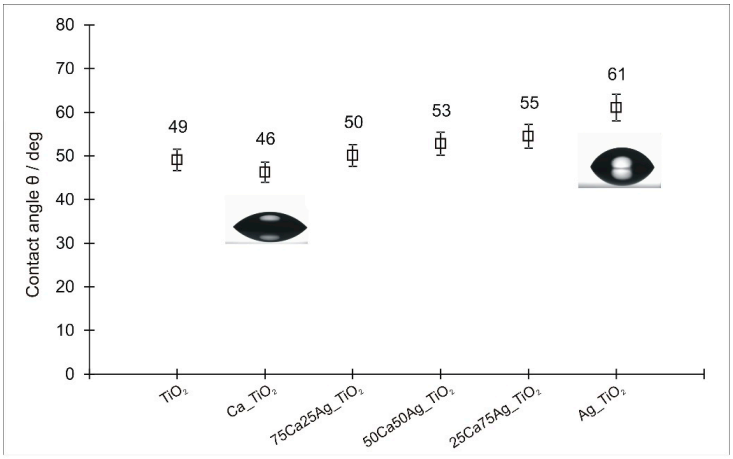

Figure 7. Contact angles Θ of the titania-based coatings on M30NW alloy samples depending on doped ions.

The TiO_2 and Ca_TiO_2 coatings have similar Θ values of 49° and 46°, respectively. The addition of silver ions causes an increase in the contact angle. As the content of silver ions in the coating increases, the value of the contact angle increases up to 61° for the highest Ag content. On the basis of wetting measurements, it was found that the surface free energy decreases with increasing concentration of silver ions in the coatings (Figure 8).

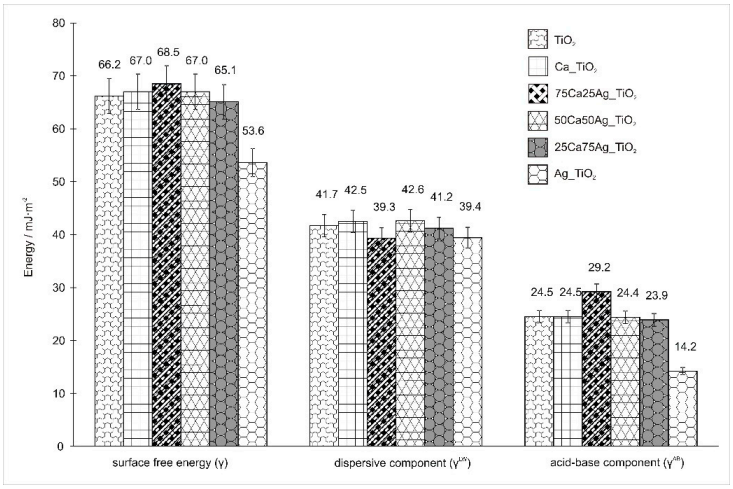

Figure 8. Surface free energy γ values (with distinction between dispersive and polar components) of the titania-based coatings doped with Ca and Ag ions in different molar ratios.

As it is known, the surface free energy (γ) is a sum of the dispersive (γ^{LW}) and acid-base (γ^{AB}) components (Equation (4)), which both determine this value.

$$\gamma = \gamma^{LW} + \gamma^{AB}. \quad (4)$$

Figure 8 gives the values of the γ, with distinction between polar (γ^{AB}) and dispersive (γ^{LW}) components. In our study, the surface free energy value is mainly influenced by the γ^{AB} component, since the value of the γ^{LW} component is similar for all surfaces and amounts ca. 40 mJ/m^2. It can be clearly seen that both surface free energy γ and its polar component γ^{AB} decrease with increasing Ag concentration in the coatings. It is related to the formation of silver oxide particles on the surface of the coatings. Silver atoms present on the coatings' surface are exposed to the atmosphere and are free to bond with other atoms, especially with oxygen and water [46]. Therefore, as the concentration of silver

in the coating increases, the number of Ag-O bonds increases, which, in consequence, changes the properties of surface.

It can be concluded that all investigated TiO_2-based coatings are hydrophilic regardless of the type and molar ratio of the dopants. The higher surface wettability results in better adhesion and proliferation of the eukaryotic cells [47]. That can be beneficial for biological applications, especially for use in the circulatory system. According to the literature [48], the hydrophilic titania coating reduces adsorption of proteins and minimizes adherence of blood platelets on the surface.

3.5. Biological Evaluation: Cell Viability and Proliferation Ability Assays

Figure 9a presents the results obtained from the live/dead test and the determined amounts of cells viability after direct contact with the examined surfaces. The highest amount of live cells (i.e., above 98%) was observed for the sample 50Ca50Ag_TiO_2. The biggest percentage of dead cells was noted for the sample 25Ca75Ag_TiO_2 (~22% of all collected cells). Statistical significance on the level of $p < 0.05$ was noted between sample 25Ca75Ag_TiO_2 and TiO_2, Ag_TiO_2, 75Ca25Ag_TiO_2 for live cells as well as for the dead ones. Nevertheless, none of the examined materials is cytotoxic. All the samples fulfill the requirements defined in the ISO 10993-5—the viability is above 70%. That states that prepared sol-gel coatings, regardless of doped element—Ca, Ag or their mixture—are biocompatible materials. Taking into consideration the average amount of cells, in the case of a cells' proliferation (Figure 9b), it was observed that the trend of obtained results is similar to the trend for results obtained for contact angle measurement. It can be stated also that cells' proliferation slightly increases with decreasing surface free energy—the highest is for Ag_TiO_2 sample, which has the lowest γ values. Calcium addition does not influence the cells, most proliferate onto the samples doped only with Ag (Ag_TiO_2) and their amount is higher than for uncoated basic sample. Nevertheless there are no statistically significant differences between all evaluated coatings. It can state that, in the case of doped sol-gel coatings, their biological response depends mainly on surface topography and wettability of the samples, and to a very small extent is the effect of the content of individual elements included in the coating.

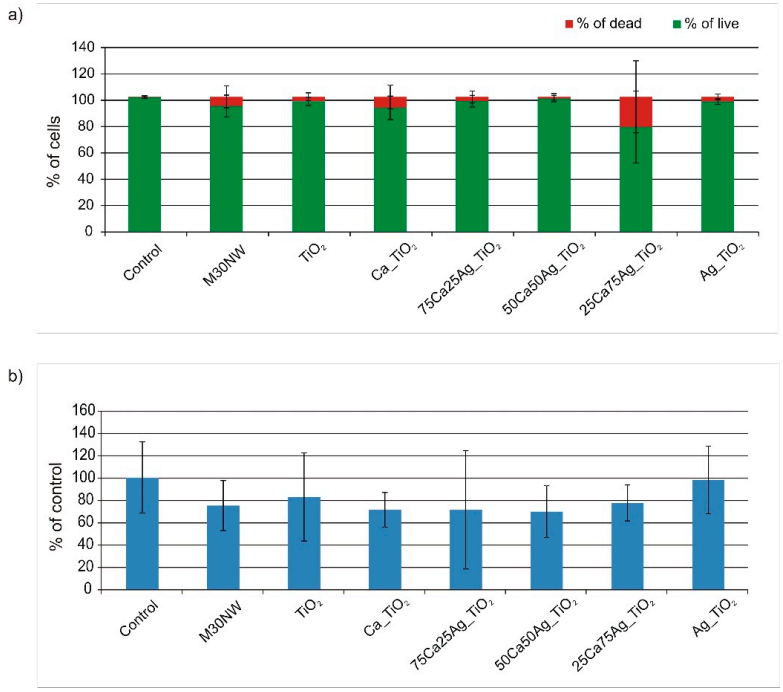

Figure 9. The results of (**a**) the live/dead test and (**b**) the cells' proliferation evaluation for all the examined coatings after 48 h of direct contact (conducted according to the protocol of ISO 10993-5: Tests for Cytotoxicity—In Vitro Methods).

The biocompatibility is usually defined as "the ability of a material to perform with an appropriate host response in a specific application" [49]. Interactions between biological system and biomaterial surface run in the following order: In the first few nanoseconds, the water molecules and proteins reach the surface, being followed by the cells [50]. The interaction of proteins and cells with the surface is driven by the specific surface features: Surface chemistry, topography, roughness, wettability, and crystallinity. Cells can sense the chemistry and topography of the surface to which they adhere. Cell behavior is different on different nanosurfaces, because nanomorphology of the material may significantly influence protein and cell adhesion. In general, cells show good spreading, proliferation, and differentiation on hydrophilic surfaces. Nevertheless, the major factor determining the nature of the cells' interaction with biomaterials is the composition and conformation of the proteins adsorbed on the surface. The adhesion and behavior of cells are affected by adsorption of serum and extracellular matrix proteins [51]. Therefore, the observed difference in the proliferation and viability of osteoblast cells may be caused by the difference in the absorption of proteins responsible for the cell colonization process. The adsorption of proteins responsible for the cell colonization and their activity may be affected by one or more interactions between proteins and surfaces, including van der Waal's interactions, electrostatic interactions, hydrogen bonding, and hydrophobic interactions [52–56]. According to the literature, generally higher surface wettability results in better adhesion and proliferation of the eukaryotic cells [57]. Although, when the surface wettability is very high, water adsorbs preferentially on the surface [58] and thus can reduce adsorption of the proteins. It has been shown by the study of Xu et al. that surfaces with $\theta > \sim 60°–65°$ show stronger adhesion forces for proteins than the surfaces with $\theta < 60°$ [57]. Generally, hydrophobic surfaces are considered to be more protein adsorbent than hydrophilic surfaces, due to strong hydrophobic interactions occurring at these surfaces [59] in direct contrast to the repulsive solvation forces arising from strongly bound water at the hydrophilic surface [53]. As proteins determine the cell proliferation results, for the sample with the highest amount of Ag having the highest contact angle (above 61°), the average number of proliferated cells is the highest—almost at the same level as a control. For the other doped samples, with the changing molar ratios of calcium ions Ca^{2+} and silver ions Ag^{+} (Ca/Ag 3:1, 1:1, 1:3) in TiO_2 sol, contact angle is on the level of ~50°–55°. The surface wettability is on a very similar level for all doped TiO_2 coatings, so the results obtained from the live/dead assay confirmed this dependence—osteoblast proliferation for all doubly-doped coatings is at the comparable level. However, it should be noted that the differences between proliferation results for all coatings are not significant and are in the range of experimental error. Therefore, it could be concluded that, in general, osteoblast cells growth is promoted on all coated surfaces, regardless of the increase of particular component elements as Ag and Ca, nor differences in nanotopography. Similarly, no morphological differences for the osteoblast-like cells were reported in the literature for the Ca-Ag coexisting nano-structured titania layer on Ti metal surface [34], as well as for Ag-Sr co-doped hydroxyapatite/TiO_2 nanotube bilayer coatings [33]. These reports prove that incorporating a secondary bioactive compound (e.g., Ca or Sr ions) not only improves bioactivity of the coating, but it is also effective in lessening Ag cytotoxicity and optimally preserving its antibacterial properties.

According to T.T Liao el at. [60], less ordered phases in a coating results in a lower adsorption of proteins and cells on the surface, while increasing crystallinity of the coating improves cell colonization. For the coatings examined in this work, the XRD results showed that the crystallinity of the anatase in TiO_2 coating increases with increasing amount of Ag and the highest was obtained for the Ag_TiO_2 sample. At the same time, for this sample, the highest value of R_q = 7.88 nm was observed. Surface topography plays an important role in providing three-dimensionality of cells [61]. For instance, the topography of the collagen fibers, with repeated 66 nm binding, has shown to affect cell shape [62]. Focal adhesion interacting with the surface is established by cell filopodia (which are 0.25–0.5 μm wide and 2–10 μm long) [63]. Filopodia can interact with the surface due to surface features, which are either arranged randomly or in some geometrical order and have dimensions from the micro to the nanometer range [61]. Beyond micrometers, it has been shown that nanometric (1–500 nm) features

can elicit specific cell responses [61,62]. In case of our experiment, as the surfaces of the coatings show different nanostructures, we noted that osteoblast cells react differently on the surface revealing dissimilar morphology (Figure 10). The results we got are consistent with the observations made by S. Lee et al. [64]. In their results they noticed that as micropore size increases, cell number is reduced and cell differentiation and matrix production is increased. Their study demonstrated that the surface topography plays an important role for phenotypic expression of the MG63 osteoblast-like cells. In our case, we observed that cell shape and proliferation level are different as the coatings' topography in nanoscale is different. For most porous surfaces (Ca_TiO_2, 75Ca25Ag_TiO_2) we observed fewer cells and increased matrix production, although their number is still relatively high. For surfaces without pores, osteoblasts are more elongated (more natural morphology), although other factors decrease their number compared to control.

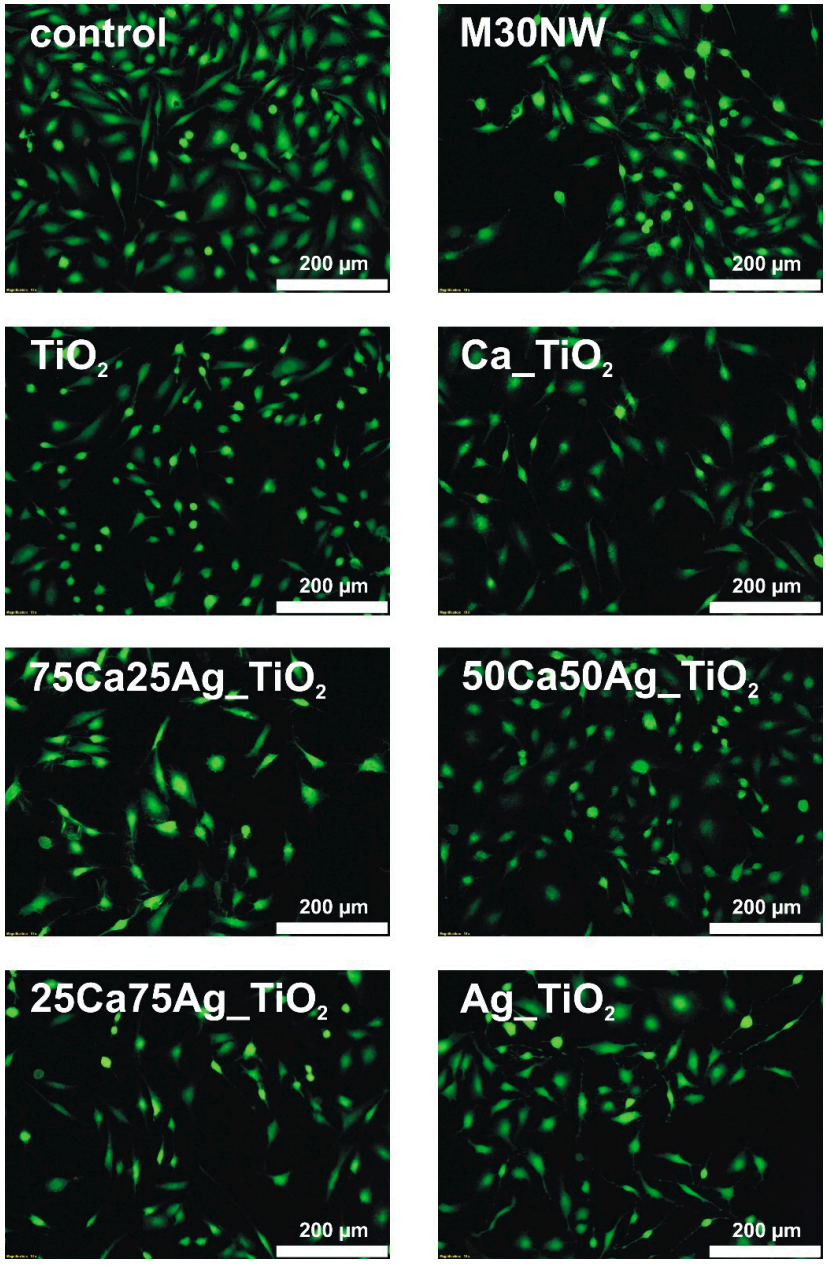

Figure 10. The osteoblast cells images (fluorescent stained, live cells—green colour, bar 200 µm) after 48 h of growing on samples (direct contact) modified by coatings with different composition and nanostructure.

4. Conclusions

Application of the sol-gel method made it possible to obtain homogeneous titanium dioxide coatings co-doped with calcium and silver ions in a different molar ratio. The thermal treatment at 450 °C allowed crystalline coatings of anatase structure to be obtained at a thickness of approx. 70–80 nm, regardless of the amount of each dopant. It was found that the amount of crystalline anatase phase increases with increasing silver content. All sol-gel TiO_2-based coatings investigated in this study have hydrophilic properties regardless of the type of dopant. Thus, each of the produced coatings is beneficial to the adsorption of osteoblast cells and thus for bone-bonding properties of implants. The doping with calcium and silver ions affects the topography of the TiO_2-based coatings. Undoped coatings and coatings doped only with calcium ions are characterized by small surface development. Along with the increase of silver content in the coating, its surface development increases as well, due to pores existing in the coating. The corrosion tests confirmed anticorrosive properties of TiO_2-based coatings. The best protective (anticorrosive) properties were registered for the coating doped with calcium ions. Analysis of corrosion results showed that the increase in silver content resulted in increasing of the electrochemical activity of the investigated samples in PBS solution. The immersion test in the SBF solution confirmed the bioactivity of the tested coatings—the apatite layer was found on the samples' surface. It was found that, with the increase in calcium ion content in the coating, the Ca/P ratio increases and approaches the value of 1.67, characteristic of stoichiometric hydroxyapatite.

Silver is recognized as an antibacterial element, but at the same time can be also cytotoxic for cells. Calcium is very well known as an element that can improve the osseointegration processes. Our results showed that coatings containing Ca and Ag particles, independently of their molar ratio in TiO_2 coating, are biocompatible and do not significantly reduce the proliferation ability of the osteoblast cells, compared to the pure material, as the M30NW steel is. The lack of toxicity and viability of cells above 80% for all coatings may indicate that these doubly-doped coatings meet at least one of the requirements to define them as biocompatible materials. As the other results indicated, they may also show the ability for bone-like apatite formation and significantly improved corrosion resistance in comparison to the steel biomaterial.

Author Contributions: B.B.: Conceptualization, methodology, investigations (surface characterization and corrosion investigations), results analysis, visualization, writing, editing, and supervising the manuscript; P.O.: Resources, corrosion investigations, and data analysis; D.B. (Damian Batory): Surface characterization, data and results analysis, discussion, and editing the manuscript; M.C.: Wetting investigations, data and results analysis, discussion; M.K.: biological investigations, data analysis, and discussion; D.B. (Dorota Bociaga): Biological investigations, data and results analysis, discussion, writing, and editing the manuscript. All authors have read and agreed to the published version of the manuscript.

Funding: This research received no external funding.

Conflicts of Interest: The authors declare no conflicts of interest.

References

1. Fu, T.; Wen, C.S.; Lu, J.; Zhou, Y.M.; Ma, S.G.; Dong, B.H.; Liu, B.G. Sol-gel derived TiO_2 coating on plasma nitrided 316L stainless steel. *Vacuum* **2012**, *86*, 1402–1407. [CrossRef]
2. Velten, D.; Biehl, V.; Aubertin, F.; Valeske, B.; Possart, W.; Breme, J. Preparation of TiO_2 layers on cp-Ti and Ti6Al4V by thermal and anodic oxidation and by sol gel coating techniques and their characterization. *J. Biomed. Mater. Res.* **2002**, *59*, 18–28. [CrossRef] [PubMed]
3. Wang, G.; Li, J.; Lv, K.; Zhang, W.; Ding, X.; Yang, G.; Liu, X.; Jiang, X. Surface thermal oxidation on titanium implants to enhance osteogenic activity and in vivo osseointegration. *Sci. Rep.* **2016**, *6*, 31769. [CrossRef] [PubMed]
4. Wojcieszak, D.; Mazur, M.; Indyka, J.; Jurkowska, A.; Kalisz, M.; Domanowski, P.; Kaczmarek, D.; Domaradzki, J. Mechanical and structural properties of titanium dioxide deposited by innovative magnetron sputtering process. *Mater. Sci. Pol.* **2015**, *33*, 660–668. [CrossRef]

5. Dreesen, L.; Cecchet, F.; Lucas, S. DC magnetron sputtering deposition of titanium oxide nanoparticles: Influence of temperature, pressure and deposition time on the deposited layer morphology, the wetting and optical surface properties. *Plasma Process. Polym.* **2009**, *6*, S849–S854. [CrossRef]
6. Altmayer, J.; Barth, S.; Mathur, S. Influence of precursor chemistry on CVD grown TiO_2 coatings: Differential cell growth and biocompatibility. *RSC Adv.* **2013**, *3*, 11234–11239. [CrossRef]
7. Sobczyk-Guzenda, A.; Pietrzyk, B.; Szymanowski, H.; Gazicki-Lipman, M.; Jakubowski, W. Photocatalytic activity of thin TiO_2 films deposited using sol–gel and plasma enhanced chemical vapor deposition methods. *Ceram. Int.* **2013**, *39*, 2787–2794. [CrossRef]
8. Sobczyk-Guzenda, A.; Owczarek, S.; Fijalkowski, M.; Batory, D.; Gazicki-Lipman, M. Morphology, structure and photowettability of TiO_2 coatings doped with copper and fluorine. *Ceram. Int.* **2018**, *44*, 5076–5085. [CrossRef]
9. Zhang, Q.; Li, C. Pure anatase phase titanium dioxide films prepared by mist chemical vapor deposition. *Nanomaterials* **2018**, *8*, 827. [CrossRef]
10. Alam, M.J.; Cameron, D.C. Preparation and characterization of TiO_2 thin films by sol-gel method. *J. Sol-Gel Sci. Technol.* **2002**, *25*, 137–145. [CrossRef]
11. Piwoński, I. Preparation method and some tribological properties of porous titanium dioxide layers. *Thin Solid Film.* **2007**, *515*, 3499–3506. [CrossRef]
12. Burnat, B.; Dercz, G.; Błaszczyk, T. Structural analysis and corrosion studies on an ISO 5832-9 biomedical alloy with TiO_2 sol-gel layers. *J. Mater. Sci.: Mater. Med.* **2014**, *25*, 623–634. [CrossRef] [PubMed]
13. Owens, G.J.; Singh, R.K.; Foroutan, F.; Alqaysi, M.; Han, C.M.; Mahapatra, C.; Kim, H.W.; Knowles, J.C. Sol–gel based materials for biomedical applications. *Prog. Mater. Sci.* **2016**, *77*, 1–79. [CrossRef]
14. Carrera-Figueiras, C.; Pérez-Padilla, Y.; Estrella-Gutiérrez, M.A.; Uc-Cayetano, E.G.; Juárez-Moreno, J.A.; Avila-Ortega, A. Surface science engineering through sol-gel process. *Appl. Surf. Sci.* **2019**. [CrossRef]
15. Viitala, R.; Jokinen, M.; Peltola, T.; Gunnelius, K.; Rosenholm, J.B. Surface properties of in vitro bioactive and non-bioactive sol–gel derived materials. *Biomaterials* **2002**, *23*, 3073–3086. [CrossRef]
16. Park, J.W.; Park, K.B.; Suh, J.Y. Effects of calcium ion incorporation on bone healing of Ti6Al4V alloy implants in rabbit tibiae. *Biomaterials* **2007**, *28*, 3306–3313. [CrossRef]
17. Park, J.W.; Kim, Y.J.; Jang, J.H. Surface characteristics and in vitro biocompatibility of a manganese-containing titanium oxide surface. *Appl. Surf. Sci.* **2015**, *258*, 977–985. [CrossRef]
18. Park, J.W. Increased bone apposition on a titanium oxide surface incorporating phosphate and strontium. *Clin. Oral Implant. Res.* **2011**, *22*, 230–234. [CrossRef]
19. Anne Pauline, S.; Kamachi Mudali, U.; Rajendran, N. Fabrication of nanoporous Sr incorporated TiO_2 coating on 316L SS: Evaluation of bioactivity and corrosion protection. *Mater. Chem. Phys.* **2013**, *142*, 27–36. [CrossRef]
20. Burnat, B.; Robak, J.; Batory, D.; Leniart, A.; Piwoński, I.; Skrzypek, S.; Brycht, M. Surface characterization, corrosion properties and bioactivity of Ca-doped TiO_2 coatings for biomedical applications. *Surf. Coat. Technol.* **2015**, *280*, 291–300. [CrossRef]
21. Burnat, B.; Robak, J.; Leniart, A.; Piwoński, I.; Batory, D. The effect of concentration and source of calcium ions on anticorrosion properties of Ca-doped TiO_2 bioactive sol-gel coatings. *Ceram. Int.* **2017**, *43*, 13735–13742. [CrossRef]
22. Visai, L.; De Nardo, L.; Punta, C.; Melone, L.; Cigada, A.; Imbriani, M.; Arciola, C.R. Titanium oxide antibacterial surfaces in biomedical devices. *Int. J. Artif. Organs* **2011**, *34*, 929–946. [CrossRef] [PubMed]
23. Albert, E.; Albouy, P.A.; Ayral, A.; Basa, P.; Csik, G.; Nagy, N.; Roualdes, S.; Rouessac, V.; Safran, G.; Suhajda, A.; et al. Antibacterial properties of Ag–TiO_2 composite sol–gel coatings. *RSC Adv.* **2015**, *5*, 59070–59081. [CrossRef]
24. Cotolan, N.; Rak, M.; Bele, M.; Cör, A.; Muresan, L.M.; Milošev, I. Sol-gel synthesis, characterization and properties of TiO_2 and Ag-TiO_2 coatings on titanium substrate. *Surf. Coat. Technol.* **2016**, *307*, 790–799. [CrossRef]
25. Heidenau, F.; Mittelmeier, W.; Detsch, R.; Haenle, M.; Stenzel, F.; Ziegler, G.; Gollwitzer, H. A novel antibacterial titania coating: Metal ion toxicity and in vitro surface colonization. *J. Mater. Sci. Mater. Med.* **2005**, *16*, 883–888. [CrossRef] [PubMed]

26. Haenle, M.; Fritsche, A.; Zietz, C.; Bader, R.; Heidenau, F.; Mittelmeier, W.; Gollwitzer, H. An extended spectrum bactericidal titanium dioxide (TiO_2) coating for metallic implants: In vitro effectiveness against MRSA and mechanical properties. *J. Mater. Sci. Mater. Med.* **2011**, *22*, 381–387. [CrossRef] [PubMed]
27. Wang, Y.; Xue, X.; Yang, H. Modification of the antibacterial activity of Zn/TiO_2 nano-materials through different anions doped. *Vacuum* **2014**, *101*, 193–199. [CrossRef]
28. Pérez-Jorge Peremarch, C.; Perez Tanoira, R.; Arenas, M.A.; Matykina, E.; Conde, A.; De Damborenea, J.J.; Barrena, E.G.; Esteban, J. Bacterial adherence to anodized titanium alloy. *J. Phys. Conf. Ser.* **2010**, *252*, 012011. [CrossRef]
29. Pérez-Jorge, C.; Conde, A.; Arenas, M.A.; Pérez-Tanoira, R.; Matykina, E.; de Damborenea, J.J.; Gómez-Barrena, E.; Esteban, J. In vitro assessment of Staphylococcus epidermidis and Staphylococcus aureus adhesion on TiO_2 nanotubes on Ti–6Al–4V alloy. *J. Biomed. Mater. Res. A* **2012**, *100*, 1696–1705. [CrossRef]
30. Arenas, M.A.; Pérez-Jorge, C.; Conde, A.; Matykina, E.; Hernández-López, J.M.; Pérez-Tanoira, R.; de Damborenea, J.J.; Gómez-Barrena, E.; Esteba, J. Doped TiO_2 anodic layers of enhanced antibacterial properties. *Colloids Surf.* **2013**, *105*, 106–112. [CrossRef]
31. Choi, J.; Park, H.; Hoffmann, M.R. Combinatorial doping of TiO_2 with platinum (Pt), chromium (Cr), vanadium (V), and nickel (Ni) to achieve enhanced photocatalytic activity with visible light irradiation. *J. Mater. Res.* **2010**, *25*, 149–158. [CrossRef]
32. Zhou, J.; Zhao, L. Multifunction Sr, Co and F co-doped microporous coating on titanium of antibacterial, angiogenic and osteogenic activities. *Sci. Rep.* **2016**, *6*, 29069. [CrossRef] [PubMed]
33. Huang, Y.; Zhang, X.; Zhang, H.; Qiao, H.; Zhang, X.; Jia, T.; Han, S.; Gao, Y.; Xiao, H.; Yang, H. Fabrication of silver-and strontium-doped hydroxyapatite/TiO_2 nanotube bilayer coatings for enhancing bactericidal effect and osteoinductivity. *Ceram. Int.* **2017**, *43*, 992–1007. [CrossRef]
34. Rajendran, A.; Vinoth, G.; Nivedhitha, J.; Iyer, K.M.; Pattanayak, D.K. Ca-Ag coexisting nano-structured titania layer on Ti metal surface with enhanced bioactivity, antibacterial and cell compatibility. *Mater. Sci. Eng.* **2019**, *99*, 440–449. [CrossRef] [PubMed]
35. Lv, C.; Yang, M.; Lu, J.; Zhao, X.; Wang, G. Effect of Ca and Ag doping on structure, in-vitro mineralization, and anti-bacterial properties of TiO_2 coatings. *J. Chin. Ceram. Soc.* **2019**, *47*, 692–700.
36. Yetim, A.F.; Yildiz, F.; Alsaran, A.; Celik, A. Surface modification of 316L stainless steel with plasma nitriding. *Kov. Mater.* **2008**, *46*, 105–115.
37. Junping, Y.; Wei, L.; Keya, S. Study of Ce-modified antibacterial 316L stainless steel. *China Foundry* **2012**, *9*, 307–312.
38. Burnat, B.; Błaszczyk, T.; Leniart, A. Effects of serum proteins on corrosion behavior of ISO 5832-9 alloy modified by titania coatings. *J. Solid State Electrochem.* **2014**, *18*, 3111–3119. [CrossRef]
39. Kokubo, T.; Takadama, H. How useful is SBF in predicting in vivo bone bioactivity? *Biomaterials* **2006**, *27*, 2907–2915. [CrossRef]
40. Lide, D.R. *CRC Handbook of Chemistry and Physics*, 75th ed.; CRC Press: Boca Raton, FL, USA, 1994.
41. García-Serrano, J.; Gómez-Hernández, E.; Ocampo-Fernández, M.; Pal, U. Effect of Ag doping on the crystallization and phase transition of TiO_2 nanoparticles. *Curr. Appl. Phys.* **2009**, *9*, 1097–1105. [CrossRef]
42. *ASTM G102-89(2015)e1, Standard Practice for Calculation of Corrosion Rates and Related Information from Electrochemical Measurements*; ASTM International: West Conshohocken, PA, USA, 2015.
43. Zhang, X.; Li, M.; He, X.; Huang, X.; Hang, R.; Tang, B. Effects of silver concentrations on microstructure and properties of nanostructured titania films. *Mater. Des.* **2015**, *65*, 600–605. [CrossRef]
44. Kokubo, T. Bioactive glass ceramics: Properties and applications. *Biomaterials* **1991**, *12*, 155–163. [CrossRef]
45. Zhang, W.; Du, K.; Yan, C.; Wang, F. Preparation and characterization of a novel Si-incorporated ceramic film on pure titanium by plasma electrolytic oxidation. *Appl. Surf. Sci.* **2008**, *254*, 5216–5223. [CrossRef]
46. de Rooij, A. The Oxidation of Silver by Atomic Oxygen. *ESA J.* **1989**, *13*, 363–392.
47. Bociaga, D.; Sobczyk-Guzenda, A.; Komorowski, P.; Balcerzak, J.; Jastrzebski, K.; Przybyszewska, K.; Kaczmarek, A. Surface characteristics and biological evaluation of Si-DLC coatings fabricated using magnetron sputtering method on Ti6Al7Nb substrate. *Nanomaterials* **2019**, *9*, 812. [CrossRef] [PubMed]
48. Chun, Y.; Levi, D.S.; Mohanchandra, K.P.; Carman, G.P. Superhydrophilic surface treatment for thin film NiTi vascular applications. *Mater. Sci. Eng.* **2009**, *29*, 2436–2441. [CrossRef]
49. Williams, D.F. *Advances in Biomaterials*; Elsevier: Amsterdam, The Netherlands, 1988.

50. Junkar, I. Chapter Two—Interaction of cells and platelets with biomaterial surfaces treated with gaseous plasma. In *Advances in Biomembranes and Lipid Self-Assembly*; Iglic, A., Kulkarni, C.H., Rappolt, M., Eds.; Elsevier: Amsterdam, The Netherlands, 2016; Volume 23, pp. 25–59.
51. Keselowsky, B.G.; Collard, D.M.; García, A.J. Surface chemistry modulates fibronectin conformation and directs integrin binding and specificity to control cell adhesion. *J. Biomed. Mater. Res. Part A* **2003**, *66*, 247–259. [CrossRef]
52. Heynes, C.A.; Norde, W. Globular proteins at solid/liquid interfaces. *Colloids Surf. B: Biointerfaces* **1994**, *2*, 517–566. [CrossRef]
53. Israelachvili, J.; Wennerstrom, H. Role of hydration and water structure in biological and colloidal interactions. *Nature* **1996**, *379*, 219–225. [CrossRef]
54. Sit, P.S.; Marchant, R.E. Surface-dependent differences in fibrin assembly visualized by atomic force microscopy. *Surf. Sci.* **2001**, *491*, 421–432. [CrossRef]
55. Kidoaki, S.; Matsuda, T. Mechanistic aspects of protein/material interactions probed by atomic force microscopy. *Colloids Surf. B Biointerfaces* **2002**, *23*, 153–163. [CrossRef]
56. Xu, L.C.; Logan, B.E. Interaction forces between colloids and protein-coated surfaces measured using an atomic force microscope. *Environ. Sci. Technol.* **2005**, *39*, 3592–3600. [CrossRef] [PubMed]
57. Xu, L.C.; Siedlecki, C.A. Effects of surface wettability and contact time on protein adhesion to biomaterial surfaces. *Biomaterials* **2007**, *28*, 3273–3283. [CrossRef] [PubMed]
58. Ogwu, A.A.; Okpalugo, T.I.T.; Ali, N.; Maguire, P.D.; McLaughlin, J.A.D. Endothelial cell growth on silicon modified hydrogenated amorphous carbon thin films. *J. Biomed. Mater. Res. Part B Appl. Biomater.* **2008**, *85*, 105–113. [CrossRef]
59. Kongdee, A.; Bechtold, T.; Teufel, L. Modification of cellulose fiber with silk sericin. *J. Appl. Polym. Sci.* **2005**, *96*, 1421–1428. [CrossRef]
60. Liao, T.T.; Zhang, T.F.; Li, S.S.; Deng, Q.Y.; Wu, B.J.; Zhang, Y.Z.; Zhou, Y.J.; Guo, Y.B.; Leng, Y.X.; Huang, N. Biological responses of diamond-like carbon (DLC) films with different structures in biomedical application. *Mater. Sci. Eng.* **2016**, *69*, 751–759. [CrossRef] [PubMed]
61. Dalby, M.J.; Riehle, M.O.; Johnstone, H.; Affrossman, S.; Curtis, A.S.G. In vitro reaction of endothelial cells to polymer demixed nanotopography. *Biomaterials* **2002**, *23*, 2945–2954. [CrossRef]
62. Curtis, A.; Wilkinson, C. New depths in cell behaviour: Reactions of cells to nanotopography. *Biochem. Soc. Symp.* **1999**, *65*, 15–26.
63. Burridge, K.; Chrzanowska-Wodnicka, M. Focal adhesions, contractility, and signaling. *Annu. Rev. Cell Dev. Biol.* **1996**, *12*, 463–518. [CrossRef]
64. Lee, S.J.; Choi, J.S.; Park, K.S.; Khang, G.; Lee, Y.M.; Lee, H.B. Response of MG63 osteoblast-like cells onto polycarbonate membrane surfaces with different micropore sizes. *Biomaterials* **2004**, *25*, 4699–4707. [CrossRef]